MIT Open Access Articles

Surface Engineering of TiO2 ETL for Highly Efficient and Hysteresis-Less Planar Perovskite Solar Cell (21.4%) with Enhanced Open-Circuit Voltage and Stability

Massachusetts Institute of Technology

Surface Engineering of TiO$_2$ ETL for Highly Efficient and Hysteresis-Less Planar Perovskite Solar Cell (21.4%) with Enhanced Open Circuit Voltage and Stability

Mohammad Mahdi Tavakoli[1,2]*, Pankaj Yadav[3], Rouhollah Tavakoli[1], Jing Kong[2]*

[1]*Department of Materials Science and Engineering, Sharif University of Technology, 14588 Tehran, Iran*

[2]*Department of Electrical Engineering and Computer Science, Massachusetts Institute of Technology, Cambridge, MA 02139, USA*

[3]*Department of Solar Energy, Pandit Deendayal Petroleum University, Gandhinagar-380007, India*

* Corresponding authors: mtavakol@mit.edu (M.M. Tavakoli), jingkong@mit.edu (J. Kong)

Abstract

Interfacial studies and band alignment engineering on electron transport layer (ETL) play a key role for fabrication of high performance perovskite solar cells (PSCs). Here, we inserted an amorphous layer of SnO$_2$ (a-SnO$_2$) between the TiO$_2$ ETL and the perovskite absorber and studied on the charge transport properties of the device. The double-layer structure of TiO$_2$ compact layer (c-TiO$_2$) and a-SnO$_2$ ETL leads to modification of interface energetics, resulting in improved charge collection and decreased carrier recombination in PSCs. The optimized device based on a-SnO$_2$/c-TiO$_2$ ETL shows a maximum power conversion efficiency (PCE) of 21.4% as compared to 19.33% for c-TiO$_2$ based device. Moreover, the modified device demonstrates a maximum open circuit voltage (V_{oc}) of 1.223 V with 387 mV loss in potential, which is among the highest value reported for PSCs. In addition, the

optimized PSC depicts a negligible hysteresis, and stabilized performance measured under continuous light (AM 1.5G) and UV light illumination. The stability results show that the device on c-TiO$_2$/a-SnO$_2$ retains about 91% of its initial PCE value after 500 h light illumination, which is higher than pure c-TiO$_2$ (67%) based devices. Interestingly, using a-SnO$_2$/c-TiO$_2$ ETL the PCE loss was only 10% of initial value under continuous UV light illumination after 30 h, which is higher than that of c-TiO$_2$ based device (28% PCE loss).

Keywords: perovskite, efficiency, stability, UV stability, amorphous SnO$_2$, c-TiO$_2$

Introduction

Organohalide metal perovskite materials have attracted tremendous research attention in the past few years. These materials show an incredible progress in the field of solar cell application due to their excellent opto-electrical properties, result in a certified power conversion efficiency (PCE) of 22.7%.[1-4] This progress is originated from several techniques such as interface engineering, compositional engineering, crystal engineering, additive engineering, and passivation techniques.[5-8] However, before commercialization of perovskite solar cells (PSCs), challenges such as stability, scalability, hysteresis, and fabrication time and cost are needed to be addressed. In regard to fabrication time and cost, manufacturing planar device over conventional mesoporous structure is cheaper and faster, which is a great advantage for practical applications.[9-12] However, planar PSCs still suffer from hysteresis effect and stability issue.

Recent studies have shown a promising solution, with the use of PCBM and C60 as ETLs in planar PSCs, leading to high efficiency and hysteresis-free devices.[13,14] However, the device stability is still a big challenge by using these ETLs. In a normal device structure, TiO$_2$ is the most common compact ETL for fabrication of PSCs due to its suitable band alignment.

However, it has a relatively low electron mobility that causes insufficient charge separation at the interface with perovskite layer.[15] To overcome the limitations of TiO_2, a few strategies have been implemented, such as doping of TiO_2 with inorganic elements such as Y, Mg, Li, Zn and etc and passivation of TiO_2 surface with reduced graphene oxide and PCBM.[16-26] In fact, all of these treatments still are not enough for fabrication of an ideal planar perovskite device.

Planar PSCs with SnO_2 as ETL have recently emerged as an alternative to TiO_2. The advantages of SnO_2 ETL properties such as excellent charge extraction property, high carrier mobility, low temperature process, and suitable band alignment with perovskite absorber layer afford to improve the performance of planar PSCs.[10,12] Using SnO_2 as ETL, the typical hysteresis as well as high PCE issues can be addressed. Generally, the instability of PSC is originated from the interfaces and bulk of perovskite absorber layer.[27] The instability of PSCs due to bulk property can be solved by using the mixed cation composition by increasing the entropy of the system. However, stability concern related to PSCs interfaces is still an open task. Recently, some groups employed an interface layer between ETL and perovskite, or HTL and electrode in order to enhance the device stability under continuous light illumination.[28] One of the most significant challenges for c-TiO_2 or ZnO based devices is UV stability due to their photocatalytic properties.[22,27] Consequently, SnO_2 is an ideal candidate to address this issue because of its larger band gap. Up to now, some research groups reported planar PSCs based on SnO_2 ETL with efficiency over 21%.[29] As reported in the literature, FTO glass is rough and deposition of SnO_2 film on it is uneven including many pinholes. Thus, the device based on SnO_2 fabricated by spin coating is not reproducible.[11] In order to address this issue, some researchers applied SnO_2 film on top of c-TiO_2 layer. Based on SnO_2 (fabricated using nanocrystal or solution)/TiO_2 ETL some groups reported PCE over

20%.[11,22,30] Song *et al.* fabricated planar PSC device on amorphous TiO_2/crystalline SnO_2 ETL, resulted in a PCE of 21.1%, without reproducibility.[11] Liu *et al.* studied on the crystalline TiO_2/crystalline SnO_2 ETL for PSC device and reported a PCE of 18% for this architecture.[27] In fact, these studies are not comprehensive and there are a lot of significant issues on double layer architecture such as interface and stability, which need to be addressed.

Here, we propose an ETL, *i.e.*, an amorphous layer of SnO_2 on top of TiO_2 compact layer fabricated by solution process and perform a complete study on planar PSCs based on double layer of a-SnO_2/c-TiO_2. In this work, we have shown that the carrier transportation, band alignment, PCE, hysteresis, and stability of PSCs can be improved drastically using a-SnO_2/c-TiO_2 ETL compared with c-TiO_2 based devices. Using this architecture, planar PSC with a PCE of 21.4% with negligible hysteresis is reported. The device based on a-SnO_2/c-TiO_2 ETL shows a high V_{oc} of 1.223 V, which is among the highest *value* reported for triple A-cation perovskite device with a band gap of 1.61 eV. Moreover, the stability results of devices after 500 h under continuous light illumination show that a-SnO_2/c-TiO_2 device retains 91% of its initial PCE value, higher than that of pure c-TiO_2 device (67%). Interestingly, using an amorphous layer of SnO_2 on c-TiO_2 film, the device maintains 90% of its initial PCE under continuous UV light illumination, which is higher than that of c-TiO_2 based device (28% PCE loss). In this work, we have studied the role of a-SnO_2 in the device structure by using electrochemical impedance spectroscopy (EIS) measurement. The EIS results confirms that the presence of a-SnO_2 above c-TiO_2 decreases the carrier recombination drastically, resulting in better charge transfer and higher V_{oc}.

Result and discussions

Figure 1a shows the top-view SEM images of a-SnO$_2$ on FTO glass. As seen, a-SnO$_2$ layer exhibits no special feature due to its amorphous nature and only FTO grains are visible. The x-ray diffraction pattern of a-SnO$_2$ annealed at 170 °C, clearly depicts the amorphous nature of film, as shown in Figure 2b. Top view SEM image of triple A-cation perovskite on a-SnO$_2$ exhibits a uniform layer with the average grain size of 150 nm (Figure S2). Figure 1c and Fig. S1 show the cross-sectional SEM images of PSCs on c-TiO$_2$, a-SnO$_2$, and c-TiO$_2$/a-SnO$_2$. The planar PSCs devices fabricated in this work were structured as FTO glass/c-TiO$_2$ (a-SnO$_2$)/perovskite/Spiro-OMeTAD/Au (see Figure 1d). The detail fabrication step and procedure are explained in supporting information (SI). Herein, triple A-cation perovskite (Cs$_{0.05}$MA$_{0.15}$FA$_{0.85}$Pb(I$_{0.85}$Br$_{0.15}$)$_3$) with lead iodide excess was used as an absorber layer and was prepared by using anti-solvent method.[31] As shown in Figure 1e, the a-SnO$_2$ film on top of rough FTO glass is not uniform and as seen in some areas marked with red rectangular, the perovskite film is possibly making a direct contact with FTO glass. This may cause shunting problem across interface which will also reduce the reproducibility in device performance. To address the shunting problem, a thin layer of c-TiO$_2$ was deposited on FTO glass by using spray pyrolysis process (Figure 1c) between a-SnO$_2$ and the FTO glass. By applying c-TiO$_2$ layer, we can get benefit from the excellent charge extraction property of a-SnO$_2$ and solve the uniformity problem of a-SnO$_2$ on the surface of rough FTO glass. Additionally, by applying c-TiO$_2$, the roughness issue for FTO glass can be addressed, resulting in a more uniform and smooth a-SnO$_2$ ETL.

The UV-visible absorption and photoluminescence (PL) measurements were performed to understand the optical properties of perovskite films deposited on different ETLs. As seen in Figure 2, the UV absorption of perovskite depicts a band gap of 1.61 eV. The PL spectra of perovskite film on a-SnO$_2$ and c-TiO$_2$/a-SnO$_2$ ETLs exhibit comparable PL intensity but

much stronger quenching effect as compare to c-TiO$_2$. This PL result suggests that amorphous SnO$_2$ ETL has better charge extraction properties at ETL/Perovskite interface than that of c-TiO$_2$. Additionally, time-resolved PL spectra of perovskite films show consistent characteristics of the PL results. As seen in Figure 2b, the addition of a-SnO$_2$ on top of c-TiO$_2$ accelerates the PL decay as compared to bare c-TiO$_2$ sample. The calculated time constants for c-TiO$_2$, a-SnO$_2$, and c-TiO$_2$/a-SnO$_2$ are 18.53, 5.21, and 6.28 ns, respectively. These results can serve as additional evidence to explain the superior properties of a-SnO$_2$ and its combination with c-TiO$_2$ as ETLs. Moreover, it suggests that carrier dynamics inside the perovskite layer are closely influenced by the interface modification.

Figure 3a shows the current-voltage (*J-V*) curves measured under AM1.5G, 1 sun illumination in reverse and forward scan direction. We found that devices based on a-SnO$_2$ and c-TiO$_2$/a-SnO$_2$ ETLs show negligible hysteresis whereas c-TiO$_2$ based devices depict a significant hysteresis, which is common in the planar devices. In general, hysteresis in PSCs is mainly due to charge or ions accumulation and charge transfer imbalance at ETL/Perovskite interface. It is expected that the presence of a thin layer a-SnO$_2$ in between TiO$_2$/perovskite leads to increase in charge conductivity and decrease in interfacial defect density, results in lower hysteresis. The accumulation of ions and charges at ETLs/perovskite interfaces under dark and illumination is discussed in detail in the next section. The figures of merit for devices based on different ETLs are listed in Table 1. As we expected, the c-TiO$_2$/a-SnO$_2$ devices shows a champion PCE of 21.4% with V_{oc} of 1.169 V, J_{sc} of 23.91 mA/cm^2, and fill factor (*FF*) of 76.5%. In this regard, a-SnO$_2$, and c-TiO$_2$ based devices shows a PCEs of 20.34 and 19.33%, respectively. The extracted photovoltaic parameters from *J-V* characteristics for 10 devices are shown in Figure S3. The c-TiO$_2$/a-SnO$_2$ devices show a

6

narrow distribution of photovoltaic parameters as compared to a-SnO$_2$, and c-TiO$_2$ devices, which also indicates a better reproducibility. It is noteworthy that the average values of all photovoltaic parameters for c-TiO$_2$/a-SnO$_2$ device are higher than those of a-SnO$_2$, and c-TiO$_2$ devices. Interestingly, one of the devices based on c-TiO$_2$/a-SnO$_2$ ETL demonstrates a high V_{oc} of 1.223 V with 387 mV loss in potential, which is among the highest value reported for planar devices based on a perovskite with band gap of 1.61eV (Figure S4).[32] We believe that a better physical contact between the ETL (SnO$_2$) and perovskite, excellent charge extraction and lower recombination at interface are the reasons for the improved device perormance.[11] Figure 3b shows the steady state efficiency at maximum power point tracking (MPPT) of PSCs. The corresponding PCEs at MPP were obtained as 18.62, 20.16, 21.23% for the PSCs on c-TiO$_2$, a-SnO$_2$, and c-TiO$_2$/a-SnO$_2$, respectively. These results support the stability of PSCs under light illumination and negligible hysteresis in c-TiO$_2$/a-SnO$_2$ device. The external quantum efficiency (EQE) and integrated short-circuit current density of PSCs are presented in Figure 3c. The EQE measurements show a high photo-to-current conversion over 85% in probed ultraviolet-Visible spectrum, leading to a current density of 22.3, 23.2, 23.35 mA/cm^2 for c-TiO$_2$, a-SnO$_2$, and c-TiO$_2$/a-SnO$_2$ devices, respectively, which is in good agreement with J-V results. In addition, the environmental stability of the devices (without encapsulation) has been tested under ambient condition at a relative humidity of 50%, for more than 90 days. The results shown in Figure 3d, reveals a significantly better stability for c-TiO$_2$/a-SnO$_2$ with only 2% PCE loss after 90 days, whereas c-TiO$_2$ and a-SnO$_2$ ETLs based devices only retain 87 and 92% of their initial PCE values at the same condition. The stability result shows the beneficiary role of interface modification on device stability.

Table 1. Figure of merits for champion devices based on different ETLs with forward and backward scan directions

Sample	V_{oc}(V)	J_{sc} (mA/cm^2)	FF (%)	PCE (%)	Hysteresis index (%)	MPPT (%)
c-TiO$_2$/a-SnO$_2$-forward	1.164	23.78	76.2	21.11	1.35	21.23
c-TiO$_2$/a-SnO$_2$-backward	1.169	23.91	76.5	21.40		
a-SnO$_2$-forward	1.137	23.52	74.7	20.01	1.62	20.16
a-SnO$_2$-backward	1.142	23.45	75.8	20.34		
c-TiO$_2$-forward	1.112	22.43	74.6	18.65	3.51	18.62
c-TiO$_2$-backward	1.125	22.85	75.2	19.33		

To investigate the influence of SnO$_2$ film crystallinity on photovoltaic performance of the PSCs, 10 planar PSCs employing various SnO$_2$ films on TiO$_2$ annealed at various temperatures and for various time duration were prepared. Figure S5 shows the effect of annealing temperature on device photovoltaic parameters. The SnO$_2$ films were annealed at different temperatures, *i.e.,* 90, 130, 170, 210, 250, and 290 °C for 45 min. As seen, the SnO$_2$ film annealed at 170 °C exhibits the highest efficiency value, indicating the optimum temperature for annealing of the SnO$_2$ film. Moreover, we performed annealing measurements also with different annealing time, *i.e.*, 2, 15, 30, 45, 60, 90 min at fixed temperature of 170 °C. The obtained photovoltaics results indicate that the SnO$_2$ film is sensitive to not only temperature but also to the annealing time. As shown in Figure S6, the annealed SnO$_2$ film at 170 °C for 45 min was the best condition to achieve the maximum

efficiency. These experiments suggest that the SnO_2 layer is very sensitive to the annealing conditions.

In order to understand the role of a-SnO_2 on c-TiO_2 film on interfacial (ETLs/perovskite) energetic, the fermi levels, valence bands, and band gaps of different ETLs were estimated using ultraviolet photoelectron spectroscopy (UPS) measurements and the UV-visible transmittance. The calculated Fermi level and valence band of a-SnO_2, c-TiO_2, and a-SnO_2/c-TiO_2 ETLs from UPS measurement are shown in Figure 4a. From the UV-visible data shown in Figure 4b, the band gaps of c-TiO_2 and a-SnO_2 were 3.32 and 4.05 eV, respectively. By combining the UV-visible and UPS data, the valence and conduction bands of c-TiO_2, a-SnO_2, and a-SnO_2/c-TiO_2 ETLs were calculated, as shown in Figure 4c. The conduction bands of c-TiO_2, a-SnO_2, and a-SnO_2/c-TiO_2 ETLs were estimated about 4.3, 4.24, and 4.23 eV below vacuum, respectively. The schematics of band alignment for devices based on different ETLs are shown in Figure 4c. As seen, by adding a thin amorphous layer of SnO_2, the conduction band level of ETL is optimally adjusted with band level of perovskite absorber layer, which can facilitate a better charge extraction probability at ETL/perovskite interface in solar cell. Furthermore, a comparatively lower valance band in double layer ETL (8.28 eV) and a-SnO_2 (8.29 eV) compared to c-TiO_2 (7.62 eV) is also beneficial for blocking the holes, resulting in lower charge recombination that could improve the V_{oc} of double layer-based device.

From the obtained *J-V* results (Figure 3) and optical characteristics (Figure 2), improvement in device performance is mainly due to enhanced *FF* and V_{oc}. It is well known that a maximum *FF* and V_{oc} in solar cells is achievable with low series resistance, lower interfacial and bulk recombination, and higher shunt resistance. With an aim of to interpret the parasitic resistances, charge transfer and recombination kinetics in fabricated PSCs, impedance

spectroscopy (IS) measurements were performed under illumination and dark conditions as a function of applied bias.

The IS spectra of PSCs at Zero to V_{oc} bias are shown in Figure S7. The IS spectra with two semicircle and inductive loop in between high to low frequency transition in nyquist plot are obtained, which is generalized as a characteristic feature of efficient transport in PSCs.[33] With an increase in applied bias across PSCs, a decrease in radii of semicircle was observed. A faster rate of change in low frequency semicircle as that of high frequency was observed. The as shown IS spectra in Figure S7 were fitted with an electrical equivalent circuit shown in Figure S8. In the electrical equivalent circuit, R_s represents the series resistance due to connecting wire and DC resistance of PSCs, R_1 represents the transport resistance and associated with high frequency spectra, constant phase element (CPE_1) is due to dielectric property of absorber material, and R_{rec} and CPE_2 is associated with low frequency arc and associated with recombination phenomena.[34]

Figure 5a shows the variation of R_1 with respect to applied bias for fabricated PSCs, it was observed that R_1 of c-TiO_2/a-SnO_2 PSCs is higher than of a-SnO_2 and c-TiO_2 PSCs. It is expected that due to the amorphous nature of SnO_2, a higher value of R_1 is obtained. A larger value of R_1 also indicated a better contact between ETL and absorber layer. Moreover, compared to TiO_2 and SnO_2 based PSCs, the c-TiO_2/a-SnO_2 PSC also have lower R_s value. The value of R_s was obtained from the real magnitude of Z, where high frequency intercepts the Z axis in IS spectra. R_s of 17.5, 15 and 13±0.5Ω where obtained for c-TiO_2, a-SnO_2 and c-TiO_2/a-SnO_2 PSCs, respectively. Dark J-V characteristic in log scale is another effective method to investigate the R_s and recombination in PSCs. Figure S9 illustrates the log J-V characteristic of fabricated devices as a function of applied bias. A lower slope (shown with marked region) at high forward bias in case of c-TiO_2 and a-SnO_2 PSCs signifies higher R_s.[35]

Figure 5(b) shows the variation of R_{rec} with respect to applied bias for fabricated PSCs. The higher value of R_{rec} in case of c-TiO$_2$/a-SnO$_2$ PSCs as than that of c-TiO$_2$ and a-SnO$_2$ PSCs at same applied bias signifies the lower interfacial recombination that will cause an increase in V_{oc} of devices. Moreover, the surface recombination resistance is defined as the sum of R_1 and R_{rec}, is also found to be higher for c-TiO$_2$/a-SnO$_2$ PSCs than the c-TiO$_2$ and a-SnO$_2$ PSCs and in accordance with the enhanced V_{oc} and *FF* trend. A lower net terminal current in mid bias range (see Figure S9) confirms the lower recombination in c-TiO$_2$/a-SnO$_2$ PSCs than the c-TiO$_2$ and a-SnO$_2$ PSCs. To further understand the recombination kinetics, V_{oc} as a function of illumination was measured and shown in Figure S10 for PSCs. The ideality factor (*m*) of fabricated PSCs were obtained using the expression $Voc = \frac{m_{\Phi}k_B T}{q} \ln(\Phi_{ph})$ where k$_B$, T, q and Φ_{ph} are Boltzmann constant, device temperature, charge constant and light intensity, respectively. The *m* of 1.45, 1.42 and 1.38 were obtained for c-TiO$_2$, a-SnO$_2$ and c-TiO$_2$/a-SnO$_2$ PSCs, where a lower value attributes to lower interfacial recombination and which is consistent with the conclusion drawn from the analysis of Figure 5(b). The analysis of IS and V_{oc} *vs* illumination results depicts that the utilization of c-TiO$_2$/a-SnO$_2$ as an ETL layer will significantly suppress the recombination and improve the R$_s$ that leads to an enhanced *FF* and V_{oc}. These results are consistent with our TRPL measurement on different ETLs. As shown in Figure 2b, the PL decay time for perovskites on a-SnO$_2$ (5.21 ns) and c-TiO$_2$/a-SnO$_2$ (6.28 ns) ETLs are less than c-TiO$_2$ sample (18.53 ns), due to the reduced charge recombination in presence of a-SnO$_2$ layer.

Perovskite absorber material, being an electronic and ionic conductor, it is expected that under dark condition, mobile ion can drift and accumulate at interfaces with the influence of bias.[36] Whereas, under illumination due to higher population of electronic charge, ionic and electronic charge together accumulates at interfaces. The phenomena of charge and ion

accumulation can be easily evident from capacitance *vs* frequency (C-F) plot measured under illumination and dark.[37] The C-F results measured under dark shows that c-TiO$_2$, a-SnO$_2$ and c-TiO$_2$/a-SnO$_2$ devices have almost similar capacitance value signifying the same extend of ion accumulation at interfaces (Figure 5c). However, a-SnO$_2$ based PSCs shows a small increase in capacitance at low frequency due to difference in the interface energy between c-TiO$_2$/Perovskite and a-SnO$_2$/Perovskite interfaces. Moreover, measured C-F under illumination (Figure 5(d)), we found that as compared to c-TiO$_2$ based PSCs, the a-SnO$_2$ and c-TiO$_2$/a-SnO$_2$ PSCs exhibits a much higher low frequency capacitance, attributed to higher electronic charge or carrier densities at interface. Studies by Gottesman *et al.*[38] have shown that charge accumulation controls the V_{oc} of PSCs and thus the V_{oc} follows the trend of low frequency capacitance under illumination. The analysis of low frequency capacitance is in good agreement with the obtained V_{oc} trend shown in Figure 3. Moreover, Mott-Schoctky measurements as a function of applied bias were performed for the fabricated devices and shown in Figure S11. The doping density of perovskite absorber material was calculated from the slope measured at high forward bias. A doping density in the order of 10^{16}/cm^3 were observed for fabricated PSCs and in consistent with the previous reported values.[37] An almost same doping density in devices signifies that the improvement in device characteristics is due to interface phenomena rather than bulk. The characterization results of PSC device on c-TiO$_2$/a-SnO$_2$ as compared to its counterparts show the potency of this architecture for fabrication of highly efficient solar cell, which is mainly due to the synergetic effect of c-TiO$_2$/a-SnO$_2$ ETL. This was supported by PL emission, UPS measurement and capacitance *vs* frequency (C-F) plot measured under dark and light conditions.

In order to study the role of additional a-SnO$_2$ layer for practical application, stability of devices under fully light illumination were measured. This measurement was performed at

room temperature for 500 h under AM 1.5G condition. The stability results for different ETLs are shown in Figure 6a. As seen, the PCE loss for devices based on c-TiO$_2$ and c-TiO$_2$/a-SnO$_2$ were 33 and 9 % of their initial PCE values, respectively, demonstrating the role of a-SnO$_2$ interface layer. The stability of a PSC device is depended on various parameters such as operating temperature, illumination level, humidity, the intrinsic property of perovskite absorber layer, and the charge collecting layer and electrodes. All these factors need to be optimized for fabrication of stable PSC devices. As reported in the literature[10,39], it is shown that after replacing TiO$_2$ by SnO$_2$, spiro-OMeTAD by other polymers or inorganic HTLs, and using additional interface layers between HTL and back electrode can improve the stability of a PSC device significantly. For instance, one of the main problem in PSCs for stability issue is ion migration (gold and iodine) between the perovskite and back contact through HTL. In this regard, using of an inorganic HTL or an additional layer in between such as reduced graphene oxide[40] can solve this stability issue. In the present study, the improvement in stability of c-TiO$_2$/a-SnO$_2$ device is mainly due to the suppression in carrier recombination at the interface of perovskite and ETL, specially under continuous light illumination. However, still a small decrease in PCE of c-TiO$_2$/a-SnO$_2$ devices is observed after 500 h which could be due to the inherent deterioration of perovskite absorber layer or migration of Au metal into spiro-OMeTAD HTL.

Besides, the stability of devices under continuous UV light illumination was also investigated. The devices were exposed to the UV lamp in a dry air box for 30 h and measured after each 3 h. Figure 6b shows that c-TiO$_2$ based device performance decayed at a faster rate than that of c-TiO$_2$/a-SnO$_2$ devices. In fact, c-TiO$_2$ film contains many oxygen vacancies at the interface by applying UV light for long time, which may react with oxygen in the environment. Upon oxygen desorption on the surface of c-TiO$_2$, electrons could be

generated at the interface. These electrons can rapidly recombine with the hole in the valence band of perovskite, resulting in faster interfacial charge recombination. Consequently, a thin layer of a-SnO$_2$ film could shield the charge transfer passes and improve the stability of device under UV light.[40] Consequently, the interface engineering of PSC device is of crucial for fabrication highly efficient and stable PSC. Architectural design of PSC device such as double layer ETL could be an effective way for this purpose.

Conclusions

In summary, we modified the surface of TiO$_2$ ETL by applying a thin layer of amorphous SnO$_2$ for fabrication efficient planar PSCs. We showed that this interface layer not only increases the device performance but also improves the stability of the PSC devices. Our characterization results demonstrated that a-SnO$_2$ layer enhances the charge extraction properties of ETL and adjusts the band alignment of ETL with triple A-cation PSC properly, resulting in a high V_{oc} of 1.223 V with 387 mV loss in potential. Based on c-TiO$_2$/a-SnO$_2$, a planar PSC device with PCE of 21.4% was achieved with negligible hysteresis, which is among the highest PCE reported till now. Moreover, the c-TiO$_2$/a-SnO$_2$ device showed a PCE loss about 9% under continuous light illumination after 500 h, whereas this value was 33% for c-TiO$_2$ based device. Besides, it was discovered that the c-TiO$_2$/a-SnO$_2$ device indicates a good stability under the UV light, where the device retained 90% of the initial PCE after 30 h exposure to the UV light, while the c-TiO$_2$ device maintained only 72% of its performance. In addition to these results, the behavior of each ETL was further confirmed by EIS measurement, indicating the lower carrier recombination and higher V_{oc} in double layer planar device.

Acknowledgement

References

[1] National Center for Photovoltaics (NCPV) at the National Renewable Energy Laboratory (NREL); www.nrel.gov/pv/assets/images/efficiency-chart.png.

[2] J. W. Lee, H. S. Kim, N. G. Park, *Acc. Chem. Res.* **2016**, *49*, 311.

[3] W. S. Yang, B. W. Park, E. H. Jung, N. J. Jeon, Y. C. Kim, D. U. Lee, S. S. Shin, J. Seo, E. K. Kim, J. H. Noh, S. I. Seok, *Science* **2017**, *356*, 1376.

[4] M. M. Tavakoli, K. H. Tsui, Q. Zhang, J. He, Y. Yao, D. Li, Z. Fan, *ACS Nano* **2015**, *9*, 10287-10295.

[5] N. J. Jeon, J. H. Noh, W. S. Yang, Y. C. Kim, S. Ryu, J. Seo, S. I. Seok, *Nature* **2015**, *517,* 476.

[6] M. M. Tavakoli, R. Tavakoli, Z. Nourbakhsh, A. Waleed, U. S. Virk, Z. Fan, *Adv. Mater. Interfaces* **2016***,3,*1500790.

[7] N. Y. Nia, M. Zendehdel, L. Cinà, F. Matteocci, A. Di Carlo, *J. Mater. Chem. A* **2018**, *6,* 659-671.

[8] T. Li, Y. Pan, Z. Wang, Y. Xia, Y. Chen, W. Huang, *J. Mater. Chem. A* **2017***, 5*, 12602-12652.

[9] Q. Jiang, L. Zhang, H. Wang, X. Yang, J. Meng, H. Liu, Z. Yin, J. Wu, X. Zhang, J. You, *Nat. Energy* **2016**, *2*, 16177.

[10] E. H. Anaraki, A. Kermanpur, L. Steier, K. Domanski, T. Matsui, W. Tress, M. Saliba, A. Abate, M. Grätzel, A. Hagfeldt, J. P. Correa-Baena, *Energy Environ. Sci.* **2016**, *9*, 3128-3134.

[11] S. Song, G. Kang, L. Pyeon, C. Lim, G. Y. Lee, T. Park, J. Choi, *ACS Energy Lett.* **2017**, *2,* 2667-2673.

[12] J. P. C.Baena, L. Steier, W. Tress, M. Saliba, S. Neutzner, T. Matsui, F. Giordano, T. J. Jacobsson, A. R. S. Kandada, S. M. Zakeeruddin, A. Petrozza, *Energy Environ. Sci.* **2016**, *8*, 2928-2934.

[13] K. Wojciechowski, T. Leijtens, S. Siprova, C. Schlueter, M. T. Hörantner, J. T. W. Wang, C. Z. Li, A. K. Y. Jen, T. L. Lee, H. J. Snaith, *J. Phys. Chem. Lett.* **2015**, *6,* 2399-2405.

[14] H. Yoon, S. M. Kang, J. K. Lee, M. Choi, *Energy Environ. Sci.* **2016**, *9*, 2262-2266.

[15] W. Ke, G. Fang, J. Wang, P. Qin, H. Tao, H. Lei, Q. Liu, X. Dai, X. Zhao, *ACS Appl. Mater. Interfaces* **2014**, *6,* 15959–15965.

[16] K. Manseki, T. Ikeya, A. Tamura, T. Ban, T. Sugiura, T. Yoshida, *RSC Adv.* **2014**, *4,* 9652–9655.

[17] G. S. Han, H. S. Chung, B. J. Kim, D. H. Kim, J. W. Lee, B. S. Swain, K. Mahmood, J. S. Yoo, N. -G. Park, J. H. Lee, H. S. Jung, *J. Mater. Chem. A* **2014**, *3,* 9160–9164.

[18] M. M. Tavakoli, A. Simchi, Z. Fan, H. Aashuri, *Chem. Commun.* **2016**, *52,* 323-326.

[19] P. Qin, A. L. Domanski, A. K. Chandiran, R. Berger, H. -J. Butt, M. I. Dar, T. Moehl, N. Tetreault, P. Gao, S. Ahmad, M. K. Nazeeruddin, M. Grätzel, *Nanoscale* **2014**, *6*, 1508–1514.

[20] T. Bu, M. Wen, H. Zou, J. Wu, P. Zhou, W. Li, Z. Ku, Y. Peng, Q. Li, F. Huang, Y. -B. Cheng, J. Zhong, *Sol. Energy* **2016**, *139*, 290–296.

[21] S. S. Shin, W. S. Yang, J. H. Noh, J. H. Suk, N. J. Jeon, J. H. Park, J. S. Kim, W. M. Seong,

S. I. Seok, *Nat. Commun.* **2015**, *6*, 7410.

[22] M. M. Tavakoli, F. Giordano, S. M. Zakeeruddin, M. Grätzel, *Nano lett.* **2018***, 18*, 2428–2434.

[23] Y. Li, Y. Zhao, Q. Chen, Y. (Michael) Yang, Y. Liu, Z. Hong, Z. Liu, Y. -T. Hsieh, L. Meng, Y. Li, Y. Yang, *J. Am. Chem. Soc.* **2015**, *137*, 15540–15547.

[24] M. M. Tavakoli, S. M. Zakeeruddin, M. Grätzel, Z. Fan, *Adv. Mater.* 2018*,* DOI: 10.1002/adma.201705998.

[25] H. Zhou, Q. Chen, G. Li, S. Luo, T. -B. Song, H. -S. Duan, Z. Hong, J. You, Y. Liu, Y. Yang, *Science* **2014**, *345*, 542–546.

[26] M. M. Tavakoli, R. Tavakoli, S. Hasanzadeh, M. H. Mirfasih, *J. Phys. Chem. C* **2016**, *120*, 19531-19536.

[27] X. Liu, T. Bu, J. Li, J. He, T. Li, J. Zhang, W. Li, Z. Ku, Y. Peng, F. Huang, Y. B. Cheng, *Nano Energy* **2018**, *44*, 34-42.

[28] Y. Hou, X. Du, S. Scheiner, D. P. McMeekin, Z. Wang, N. Li, M. S. Killian, H. Chen, M. Richter, I. Levchuk, N. Schrenker, *Science* **2017**, *358,* 1192-1197.

[29] Q. Jiang, Z. Chu, P. Wang, X. Yang, H. Liu, Y. Wang, Z. Yin, J. Wu, Z. Zhang, J. You, *Adv. Mater.* **2017**, *29*, 1703852.

[30] Y. H. Lee, S. Paek, K. T. Cho, E. Oveisi, P. Gao, S. H. Lee, J. S. Park, Y. Zhang, R. Humphry-Baker, A. M. Asiri, M. K. Nazeeruddin, *J. Mater. Chem. A.* **2017**, *5*, 12729-12734.

[31] M. M. Tavakoli, D. Bi, L. Pan, A. Hagfeldt, S. M. Zakeeruddin, M. Grätzel, *Adv. Energy Mater.* **2018**, DOI:10.1002/aenm.201800275.

[32] N. K. Noel, M. Congiu, A. J. Ramadan, S. Fearn, D. P. McMeekin, J. B. Patel, M. B. Johnston, B. Wenger, H. J. Snaith, *Joule* **2017**, *1,* 328-343.

[33] E. Ghahremanirad, A. Bou, S. Olyaee, J. Bisquert, *J. Phys. Chem. Lett.* **2017***, 8,* 1402-1406.

[34] I. Zarazua, S. Sidhik, T. Lopez-Luke, D. Esparza, E. De La Rosa, J. Reyes-Gomez, I. Mora-Sero, G. Garcia-Belmonte, *J. Phys. Chem. Lett.* **2017**, *8,* 6073–6079

[35] P. Yadav, M. H. Alotaibi, N. Arora, M. I. Dar, S. M. Zakeeruddin, M. Grätzel, *Adv. Funct. Mater.* **2018**, 10.1002/adfm.201706073.

[36] H. S. Kim, I. Mora-Sero, V. Gonzalez-Pedro, F. Fabregat-Santiago, E. J. Juarez-Perez, N. G. Park, J. Bisquert, *Nat. Commun.* **2013**, *4*, 2242.

[37] P. Yadav, M. I. Dar, N. Arora, E. A. Alharbi, F. Giordano, S. M. Zakeeruddin, M. Grätzel, *Adv. Mater.* **2017***, 29*, 1701077.

[38] R. Gottesman, P. Lopez-Varo, L. Gouda, J. A. Jimenez-Tejada, J. Hu, S. Tirosh, A. Zaban, J. Bisquert, *Chem*, **2016**, *1,* 776-789.

[39] N. Arora, M. I. Dar, A. Hinderhofer, N. Pellet, F. Schreiber, S. M. Zakeeruddin, M. Grätzel, *Science* **2017**, DOI: 10.1126/science.aam5655.

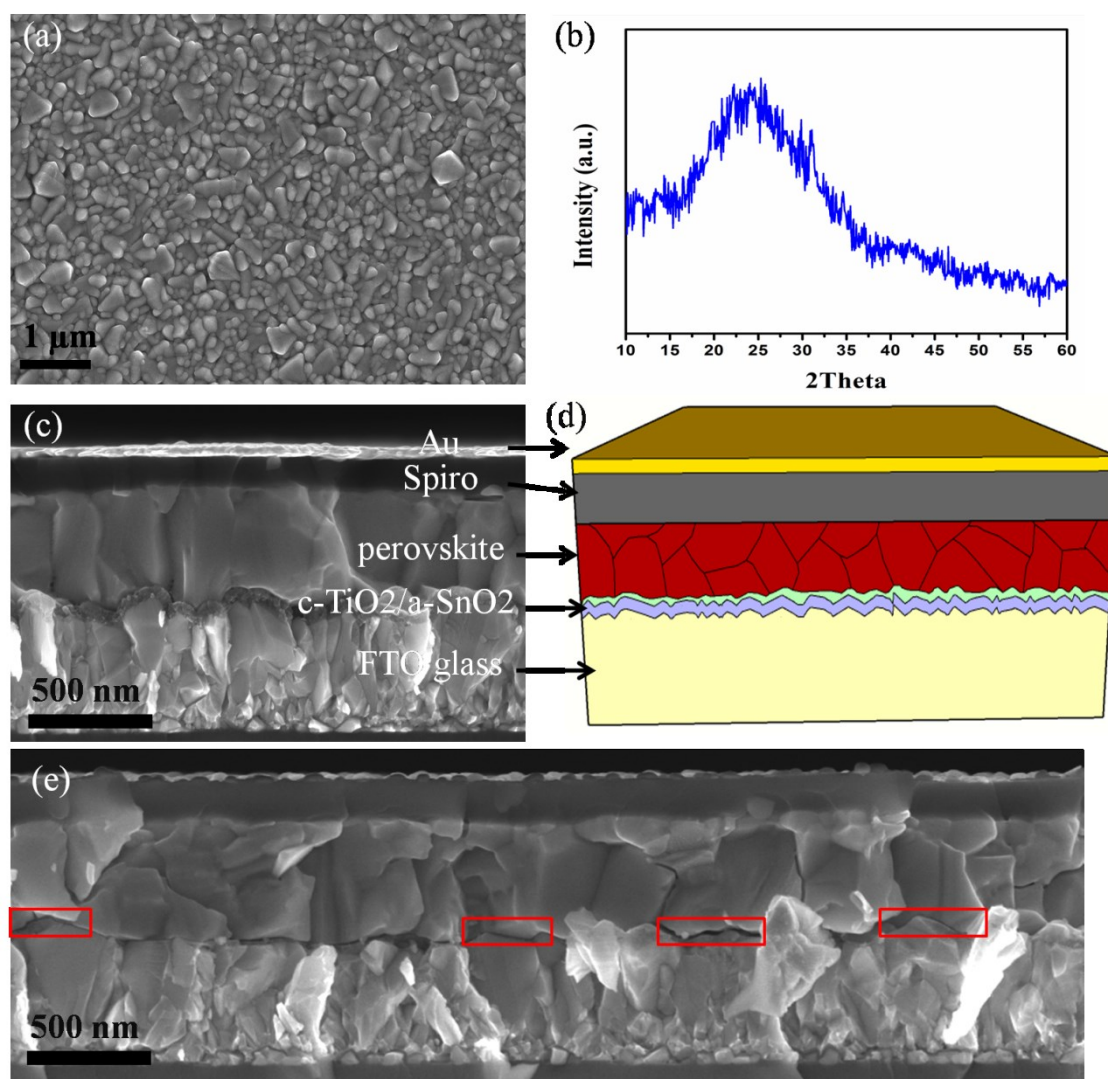[40] T. Leijtens, G. E. Eperon, S. Pathak, A. Abate, M. M. Lee, H. J. Snaith, *Nat. Commun.* **2013**, *4*, 2885.

Figure 1. (a) Top view SEM image of a-SnO$_2$ on FTO glass. Notable, a-SnO$_2$ is transparent and the grains are belonged to the FTO glass. (b) XRD pattern for amorphous phase of SnO$_2$ film deposited by spin-coating method and annealed at 170 °C. (c) Cross sectional view SEM image of c-TiO$_2$/ a-SnO$_2$ ETL. (d) Schematic of device structure. (e) Cross section SEM image of device on a-SnO$_2$ indicating some areas (red rectangular) that perovskite layer is in direct contact with the FTO glass.
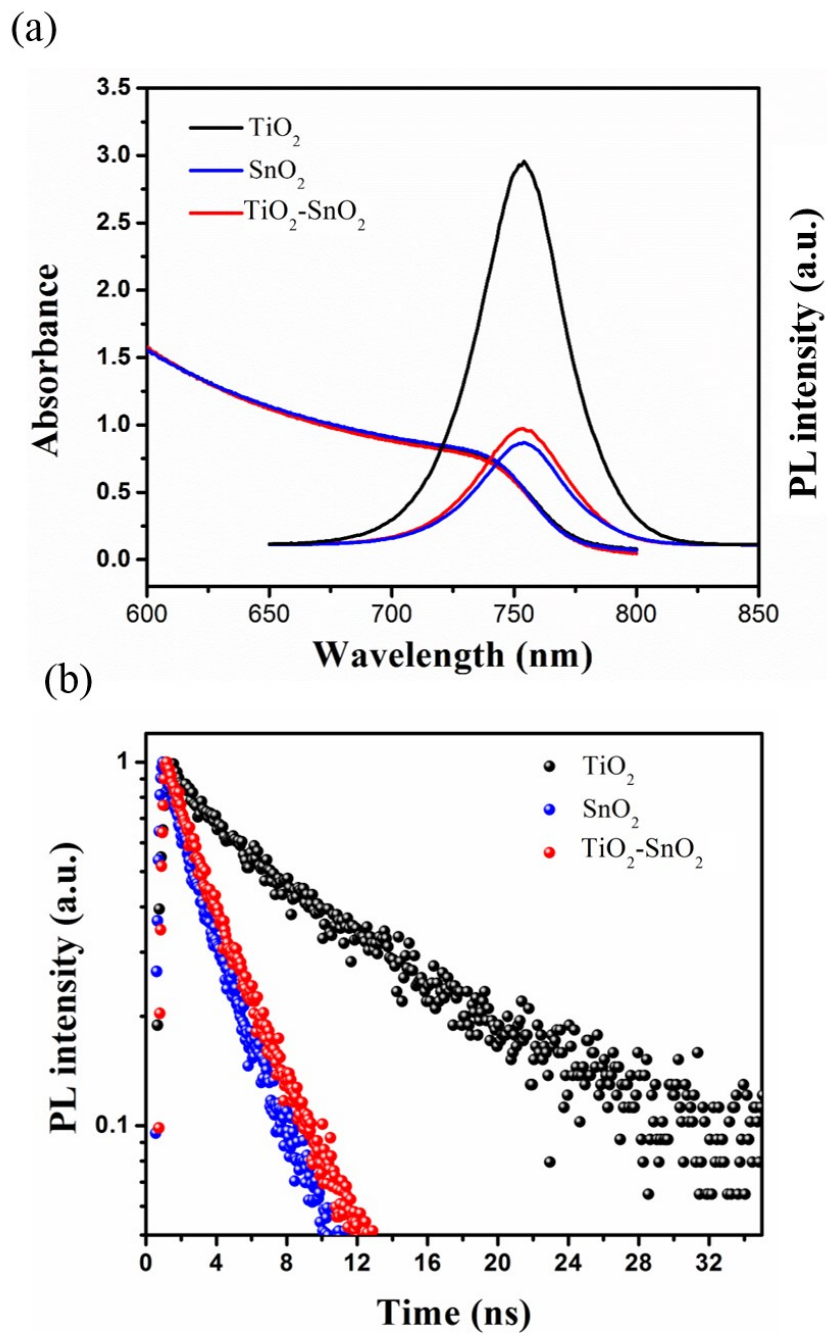
Figure 2. Optical measurement of perovskite film deposited on different ETLs; TiO_2, SnO_2, and SnO_2/TiO_2, (a) UV-visible and PL spectra, (b) time-resolved PL curves.
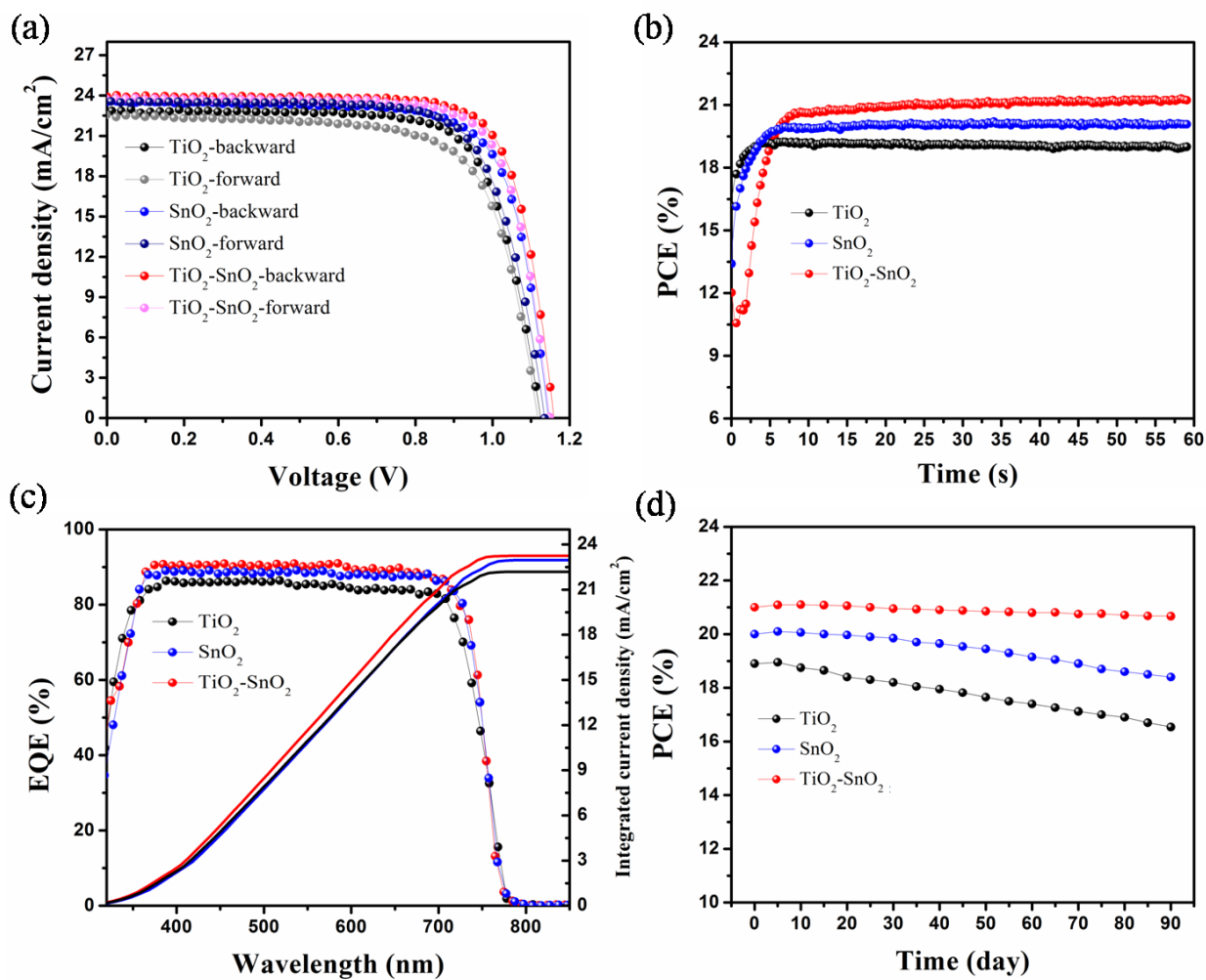
Figure 3. (a) *J-V* curves, (b) maximum power point tracking (MPPT), (c) external quantum efficiency (EQE) spectra, and (d) stability test of PSCs based on c-TiO$_2$, a-SnO$_2$, and c-TiO$_2$/a-SnO$_2$ ETLs.
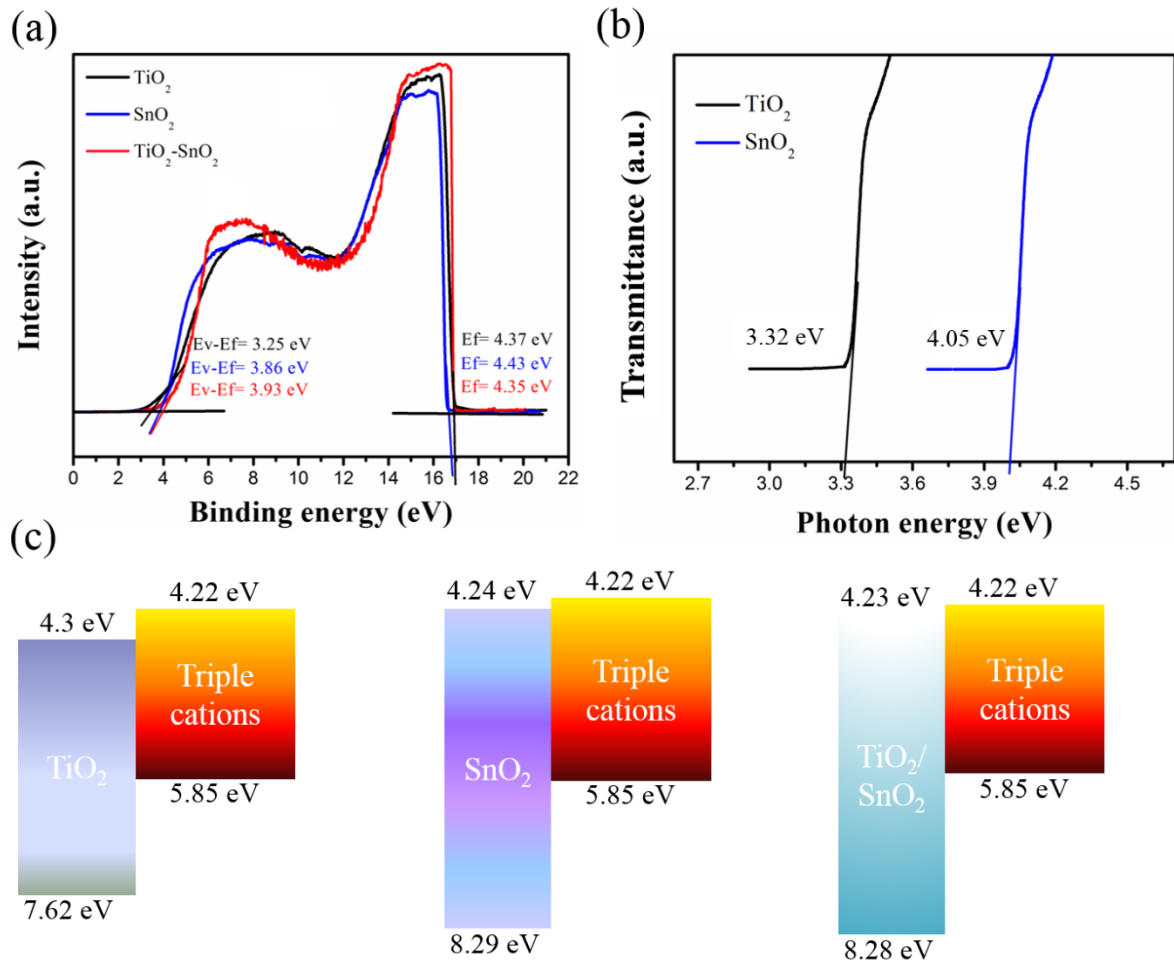
Figure 4. (a) UPS measurements of a-SnO$_2$ and c-TiO$_2$ films on Si substrate for band levels calculation. (b) Transmittance spectra of a-SnO$_2$ and c-TiO$_2$ on glass substrate. (c) Schematics of band alignment for devices based on c-TiO$_2$, a-SnO$_2$, and a-SnO$_2$/c-TiO$_2$ ETLs.
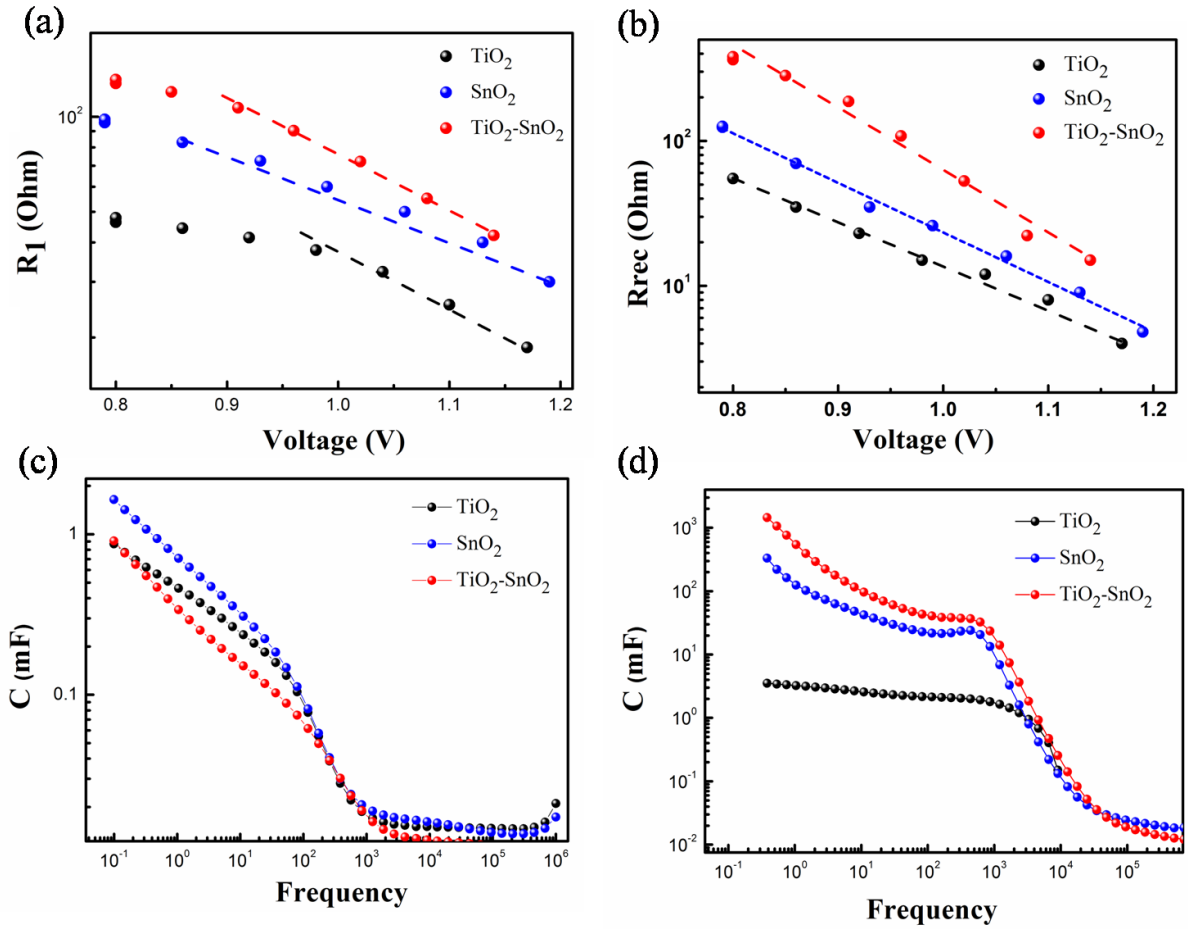
Figure 5. (a) High frequency resistance and (b) Low frequency resistance extracted from nyquist spectra by using electrical equivalent circuit for a-SnO_2 and c-TiO_2 and c-TiO_2/a-SnO_2 PSCs. (c) capacitance *vs* frequency (C-F) plot measured under dark and (d) C-F plot measured under illumination.
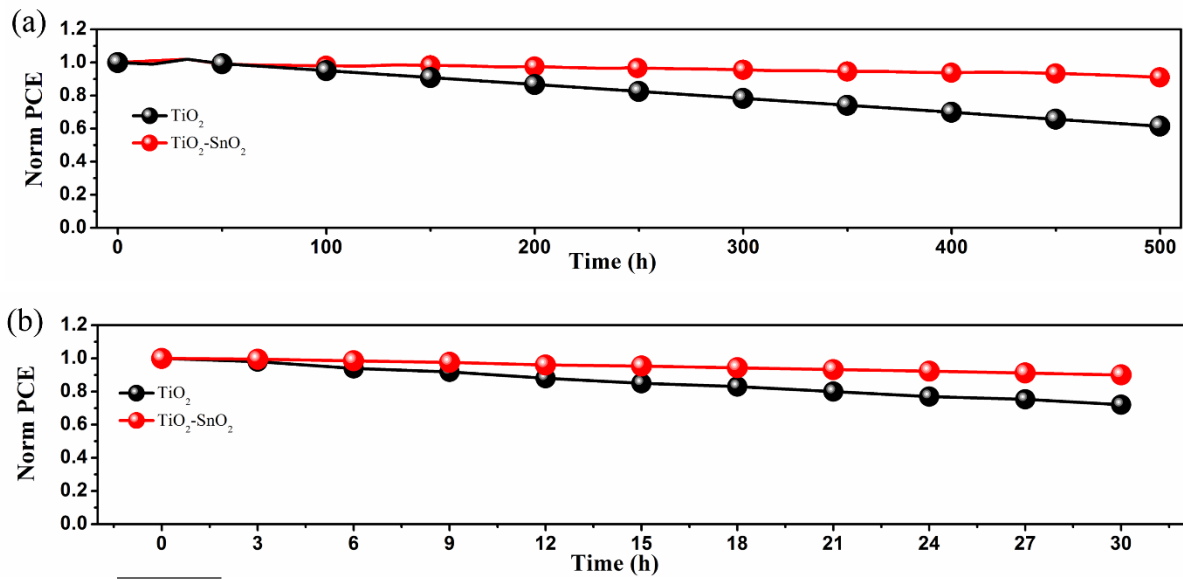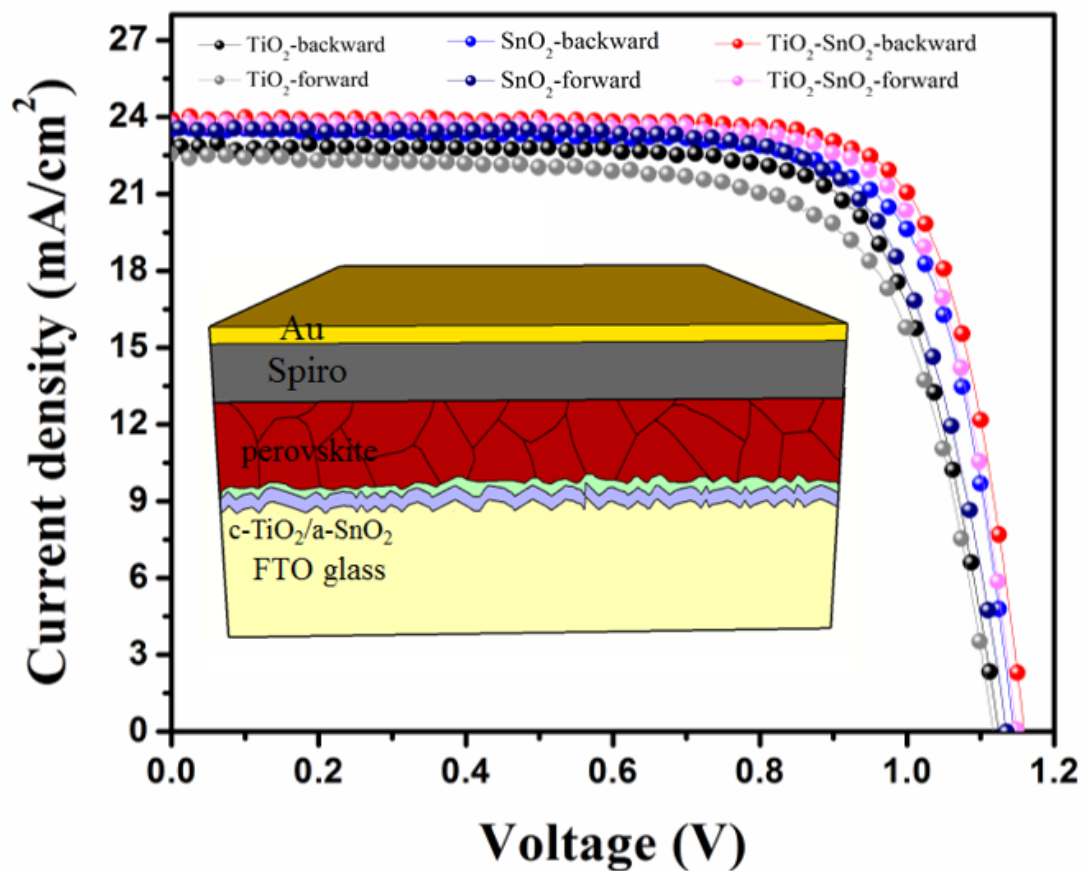
Figure 6. (a) Stability test of perovskite device on TiO_2 and SnO_2/TiO_2 ETLs under continuous light illumination at room temperature, and (b) UV stability of these devices under continuous UV light illumination inside a dry air box.

TOC graphic

The presence of an amorphous SnO_2 layer on top of the crystalline compact TiO_2 ETL mitigates the charge carrier recombination at the interface of perovskite/ETL and results in highly efficient planar perovskite solar cells with enhanced open circuit photovoltage and stability.